Enhanced Spectral Sensitivity from Ruthenium(II) Polypyridyl Based Photovoltaic Devices

Robert Argazzi and Carlo A. Bignozzi*

Dipartimento di Chimica dell' Universita, Centro di Studio su Fotoreattivita e Catalisi CNR, 44100 Ferrara, Italy

Todd A. Heimer, Felix N. Castellano, and Gerald J. Meyer*

Department of Chemistry, The Johns Hopkins University, Baltimore, Maryland 21218

Received March 2, 1994[⊗]

Ruthenium polypyridyl compounds, *cis*-[4,4′-$(CO_2H)_2$-2,2′-bipyridine]$_2$Ru$(X)_2$ and *cis*-[5,5′-$(CO_2H)_2$-2,2′-bipyridine]$_2$Ru$(X)_2$ where X = Cl^-, CN^-, and SCN^-, have been prepared, spectroscopically characterized, and anchored to high surface area TiO_2 electrodes for the conversion of visible light into electricity. Vibrational studies reveal a surface ester linkage and indicate that the sensitizers bind to TiO_2 through a distribution of interfacial interactions in a similar manner. When operating in a photoelectrochemical cell, these materials convert visible photons into electrons. Transition metal sensitizers based on the 5,5′-$(CO_2H)_2$-2,2′-bipyridine ligand generally enhance photon-to-current efficiencies at low photon energies. Consistent with a previous report, photoanodes based on *cis*-[4,4′-$(CO_2H)_2$-2,2′-bipyridine]$_2$Ru$(NCS)_2$ are the most efficient under simulated sunlight (Gratzel, M., et al. *J. Am. Chem. Soc.* **1993**, *115*, 6382). The observation of an electric field dependent luminescence indicates that radiative recombination of the dye competes with photocurrent production in some cases. A lower limit for the rate of interfacial electron injection is estimated to be $k_{et} \sim 5 \times 10^7\ s^{-1}$. A lower photocurrent efficiency observed for sensitizers based on 5,5′-$(CO_2H)_2$-2,2′-bipyridine stems in part from less efficient electron transfer to the TiO_2 surface.

The search for efficient solar energy conversion devices continues to be an important area of research.[1] Recently, an order of magnitude increase in solar energy conversion efficiencies at dye sensitized photoelectrochemical cells has been realized.[2] This breakthrough was accomplished by attaching ruthenium polypyridyl complexes to high surface area titanium dioxide, TiO_2, electrodes. When operating as photoanodes in a photoelectrochemical cell, these materials efficiently convert visible light to electricity.[2,3] Research on artificial photosynthetic devices based on this technology provides an opportunity to directly convert light energy into electricity on a molecular level. Since it is expected that most inorganic charge transfer complexes possess unique ground and excited state properties, it is not surprising to find that solar energy conversion efficiencies are dependent on the nature of the molecular dye sensitizer.

The generally accepted model for dye sensitization of wide gap semiconductors is shown in Scheme 1.[4] In this model, an excited dye injects an electron into the semiconductor conduction band from a normal distribution of donor levels and becomes oxidized. The electron is swept to the semiconductor bulk by the surface electric field and flows through an external cell to perform useful work. The oxidized dye is reduced by an electron donor present in the electrolyte, k_4. Reduction of the oxidized donor occurs at the counter electrode and the solar cell is therefore regenerative. Radiative and nonradiative decay of the excited state, k_{-1}, and recombination of the photoinjected electron with the oxidized dye sensitizer or the oxidized electron donor, k_3, represent loss mechanisms.

Scheme 1

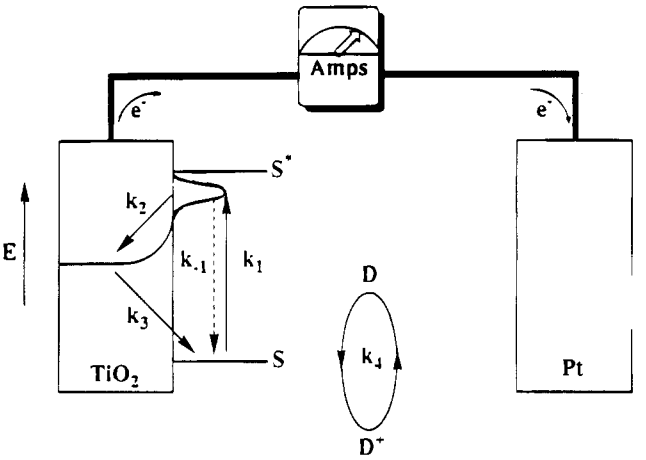

In a previous study,[3] we found that surface attached *cis*-[4,4′-$(CO_2H)_2$(2,2′-bpy)]$_2$Ru$(CN)_2$ efficiently converts photons to

[⊗] Abstract published in *Advance ACS Abstracts,* November 15, 1994.

(1) (a) Fox, M. A.; Chanon, M. *Photoinduced Electron Transfer*; Elsevier: Amsterdam, 1988. (b) Gratzel, M. *Heterogeneous Photochemical Electron Transfer*; CRC: Boca Raton, 1989.

(2) (a) Desilvestro, J.; Gratzel, M.; Kavan, L.; Moser, J.; Augustynski, J. *J. Am. Chem. Soc.* **1985**, *107*, 2988. (b) Vlachopoulos, N.; Liska, P.; Augustynski, J.; Gratzel, M. *J. Am. Chem. Soc.* **1988**, *110*, 1216. (c) Liska, P.; Vlachopoulos, N.; Nazeeruddin, M. K.; Comte, P.; Gratzel, M. *J. Am. Chem. Soc.* **1988**, *110*, 3686. (d) Amadelli, R.; Argazzi, R.; Bignozzi, C. A.; Scandola, F. *J. Am. Chem. Soc.* **1990**, *112*, 7099. (e) O'Regan, B.; Moser, J.; Anderson, M.; Gratzel, M. *J. Phys. Chem.* **1990**, *94*, 8720. (f) Desilvestro, J.; Gratzel, M.; Kavan, L.; Moser, J.; Augustynski, J. *J. Am. Chem. Soc.* **1990**, *94*, 8720. (g) O'Regan, B.; Gratzel, M. *Nature* **1991**, *353*, 737. (h) Nazeeruddin, M. K.; Kay, A.; Rodicio, I.; Humphry-Baker, R.; Muller, E.; Liska, P.; Vlachopoulos, N.; Gratzel, M. *J. Am. Chem. Soc.* **1993**, *115*, 6382. (i) Hay, A.; Gratzel, M. *J. Phys. CHem.* **1993**, *97*, 6272.

(3) Heimer, T. A.; Bignozzi, C. A.; Meyer, G. J. *J. Phys. Chem.* **1993**, *97*, 11987.

(4) (a) Gerischer, H. *Photochem. Photobiol.* **1972**, *16*, 243. (b) Gerischer, H.; Willig, F. *Top. Current Chem.* **1976**, *61*, 31. (c) Memming, R. *Prog. Surf. Sci.* **1983**, *17*, 7. (d) Gerischer, H. *Electrochim. Acta* **1990**, *35*, 1677. (e) Parkinson, B. A.; Spitler, M. T. *Electrochim. Acta* **1992**, *37*, 943 and references cited therein.

0020-1669/94/1333-5741$04.50/0

electrons while *cis*-[4,4′-$(CO_2H)_2$(2,2′-bpy)]$_2$Os$(CN)_2$ did not. The molecular level similarity of the complexes, the energetic coincidence of their excited state redox potentials, comparable absorptances, and different ground state redox potentials led us to conclude that k_3 and/or k_4 was responsible for the lower photocurrent efficiency observed with *cis*-[4,4′-$(CO_2H)_2$(2,2′-bpy)]$_2$Os$(CN)_2$/TiO_2. This conclusion is important as it signals the need for dye molecules with positive redox potentials to ensure rapid donor oxidation, k_4, and slower recombination of the conduction band electron with the oxidized dye molecule.

Metal to ligand charge transfer (MLCT) sensitizers with positive metal-based oxidation potentials have, however, the disadvantage of exhibiting high energy absorption bands which only harvest a fraction of visible light.[5] For complexes of the type *cis*-Ru$(LL)_2(X)_2$ (where LL = bidentate polypyridine ligands and X = ancillary ligands) intense MLCT absorption bands are often observed from 400 to 600 nm with negligible absorption at longer wavelengths. The MLCT absorption can be extended to lower energy by appropriate substituent changes on the chromophoric ligands or by decreasing the $d\pi-\pi^*$ back-bonding donation to the nonchromophoric ligands. The effect of these changes on the photophysical properties of metal polypyridine complexes has been the subject of several investigations[5] which have given fundamental insight into the factors which govern radiative and nonradiative decay processes of excited states.

In an attempt to extend the spectral sensitivity of dye molecules toward the red, we have designed new *cis*-Ru$(LL)_2$-$(X)_2$ polypyridyl complexes based on the ligand 5,5′-$(CO_2H)_2$-2,2′-bipyridine (hereafter abbreviated at 5,5′-(LL)), which has π^* accepting orbitals at lower energy than the corresponding 4,4′-$(CO_2H)_2$-2,2′-bipyridine (abbreviated 4,4′-(LL)). The surface attachment and photoelectrochemical properties of *cis*-[5,5′-(LL)]$_2$Ru$(X)_2$ (X = Cl^-, CN^-, SCN^-) and the corresponding 4,4′-(LL) species on TiO_2 have been investigated. The photoelectrochemical characteristics exhibited by these species are rationalized in terms of spectroscopic and photophysical properties measured in fluid solution. Enhanced spectral response at lower photon energies has been achieved with *cis*-[5,5′-(LL)]$_2$Ru$(X)_2$ (X = Cl^-, SCN^-). Of particular relevance in the context of practical applications, is the performance of *cis*-[4,4′-(LL)]$_2$Ru$(NCS)_2$ anchored to TiO_2 in a photoregenerative cell. With this complex, impressive solar energy conversion efficiencies are observed in agreement with data recently reported by Gratzel and co-workers.[2h]

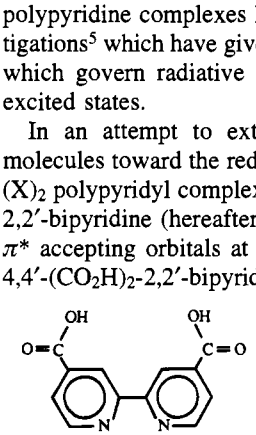

4,4′-(LL)

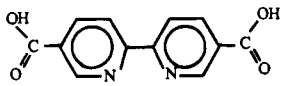

5,5′-(LL)

Experimental Section

Materials. All chemicals were reagent grade unless otherwise specified. Water was deionized with a Barnstead Nanopure System. Tetra-*n*-butylammonium hexafluorophosphate (abbreviated TBAH) (Fluka; Electrochemical grade) and 2,2′-bipyridine-4,4′-dicarboxylic acid (Aldrich) were used as received. 2,2′-Bipyridine-5,5′-dicarboxylic acid and 2,2′-bipyridine-5,5′-bis(ethoxycarbonyl) (abbreviated [5,5′-(DCE-bpy)]) were prepared by literature methods.[6] *cis*-[4,4′-(LL)]$_2$-Ru$(Cl)_2$ was prepared by the method described by Liska.[2b] *cis*-[4,4′-(LL)]$_2$Ru$(CN)_2$ was available from previous studies.[3] Spectrograde solvents were used for electrochemical and spectroscopic measurements. SiO_2 films were purchased from Analtech.

Preparations. (a) [5,5′-(LL)]$_2$Ru$(Cl)_2$. The procedure used to prepare the [5,5′-(LL)]$_2$Ru$(Cl)_2$ complex is analogous to that used to prepare [4,4′-(LL)]$_2$Ru$(Cl)_2$. A 50 mg quantity of $RuCl_3 \cdot 3H_2O$ (0.19 mmol) and 94 mg of 5,5′-(LL) (0.38 mmol) were dissolved in 10 mL of DMF and refluxed under argon for 8 h. The solution was concentrated under vacuum and cooled, and the complex was precipitated by addition of acetone−ether. The dark green solid product was filtered off and dried in air. Anal. Calcd for $C_{24}N_4O_8H_{16}Cl_2Ru$: C, 43.65; N, 8.48; H, 2.44. Found: C, 42.95; N, 8.32; H, 2.57.

(b) [5,5′-(DCE-bpy)]$_2$Ru$(Cl)_2$. A 50 mg quantity of $RuCl_3 \cdot 3H_2O$ (0.19 mmol) and 114 mg of 5,5′-(DCE-bpy) (0.38 mmol) were dissolved in 5 mL of DMF and refluxed under argon for 5 h. During this time the solution turned from brown-orange to dark green. The solution was concentrated under vacuum and cooled, and the complex was precipitated by addition of ether. The green product was recrystallized from 50% chloroform−ethanol. Anal. Calcd for $C_{32}N_4O_8H_{32}Cl_2Ru$: C, 49.75; N, 7.25; H, 4.17. Found: C, 49.33; N, 7.04; H, 4.12.

(c) [5,5′-(LL)]$_2$Ru$(CN)_2$. 50 mg of [5,5′-(LL)]$_2$Ru$(Cl)_2$ was dissolved in a minimum of water and neutralized to pH 7 by addition of sodium hydroxide. A solid was precipitated by addition of acetone, filtered off, and redissolved in 10 mL of methanol under argon, and 200 mg of NaCN (4 mmol) in 10 mL of water was added. The dark violet solution was refluxed for 3 h in the dark. During this time the solution turned orange. After evaporation to dryness, the solid was redissolved in water and the complex was precipitated at pH 2 with HCl in a well ventilated hood. The red-orange solid was filtered off, washed with water and acetone, and air dried. Anal. Calcd for $C_{26}N_6O_8H_{16}Ru \cdot 3H_2O$: C, 44.90; N, 12.08; H, 3.19. Found: C, 45.07; N, 11.46; H, 3.14.

(d) [5,5′-(LL)]$_2$Ru$(NCS)_2$. 50 mg of [5,5′-(LL)]$_2$Ru$(Cl)_2$ was dissolved in a minimum of water and neutralized to pH 7 by addition of sodium hydroxide. A solid was precipitated by addition of acetone, filtered off, and redissolved in 10 mL of methanol under argon, and 400 mg of NaNCS (4.93 mmol) in 10 mL of water was added. The solution was refluxed for 3 h in the dark under argon and then evaporated to dryness. The solid was redissolved in water and the complex precipitated at pH 2 by addition of 1 M HCl. The dark blue solid was filtered off, air dried, and recrystallized from methanol. Anal. Calcd for $C_{26}N_6S_2O_8H_{16}Ru \cdot 3H_2O$: C, 41.11; N, 11.06; H, 2.92. Found: C, 41.13; N, 10.92; H, 2.98.

(e) [4,4′-(LL)]$_2$Ru$(NCS)_2$. This dark violet complex was prepared as described for [5,5′-(LL)]$_2$Ru$(NCS)_2$, by using [4,4′-(LL)]$_2$Ru$(Cl)_2$] as a starting material.

(f) (TBA)$_4$[(5,5′-$(COO^-)_2$bpy)$_2$Ru$(X)_2$] and (TBA)$_4$[(4,4′-$(COO^-)_2$-bpy)$_2$Ru$(X)_2$] (X = CN^-, SCN^-). The tetrabutylammonium salts were prepared from the corresponding sodium salts by ion exchange chromatography with Sephadex SP C25 (Pharmacia).

Electrode Preparation. The TiO_2 electrodes were prepared using a variation of a published technique.[2g] Tin oxide coated glass electrodes (Libby Owens Ford) with a resistance of 8 Ω/square were cleaned in hexane to remove residual oils, then rinsed with EtOH and air dried. Finely divided TiO_2 particles were prepared by grinding 12 g of TiO_2 (Degussa, P25) in 4 mL of H_2O containing 0.4 mL of acetylacetone (Aldrich 99%) and 0.2 mL of Triton X-100 surfactant (Aldrich, non-UV absorbing) with a mortar and pestle. An additional 16 mL of water was slowly added with continued grinding for 10 min. Electrode substrates were secured, conductive side up, to a piece of white paper with cellophane tape. Several drops of the TiO_2 solution were distributed about the electrode surface and then spread uniformly by rolling a 1 cm diameter test tube across the electrode surface. The

(5) For reviews see: (a) Meyer, T. J. *Pure Appl. Chem.* **1986**, *58*, 1193. (b) Juris, A.; Barigelletti, F.; Campagna, S.; Balzani, V.; Besler, P.; Von Zelewsky, A. *Coord. Chem. Rev.* **1988**, *84*, 85. (c) Meyer, T. J. *Acc. Chem. Res.* **1989**, *22*, 364. (d) DeArmond, M. K.; Myrick, M. L. *Acc. Chem. Res.* **1989**, *22*, 364. (e) Yersin, H.; Braun, D.; Hensler, G.; Gallhuber, E. In *Vibronic Processes in Inorganic Chemistry*; Flint, C. D., Ed.; Kluwer Academic Publishers: Dordrecht, 1989; p 195. (f) Balzani, V.; Scandola, F. *Supramolecular Photochemistry*; Ellis Harwood: Chichester, U.K., 1990. (g) Kalyanasundaram, K. *Photochemistry of Polypyridine and Porphyrin Complexes*; Academic Press: New York, 1992; p 87.

(6) (a) Sprintschnik, G.; Sprintschnik, H. W.; Kirsh, P. P.; Whitten, D. G. *J. Am. Chem. Soc.* **1977**, *99*, 4947. (b) Elliot, C. M.; Hershenhart, E. J. *J. Am. Chem. Soc.* **1982**, *104*, 7519.

Table 1. Optical and Electrochemical Properties of Compounds in Dimethylformamide

complex[a]	$Ru^{III/II}$ [b] (V *vs* SCE)	$L^{-/0}$ [c] (V *vs* SCE)	λ_{abs}, max (nm)[d]	λ_{em}, (nm)[e]	τ (ns)[f]
$[4,4'\text{-}(LL)_2Ru(CN)_2$	0.90	−1.30*	530	733	190
$(TBA)_4[4,4'\text{-}dcb^-]_2Ru(CN)_2$			498	690	580
$[4,4'\text{-}(LL)]_2Ru(NCS)_2$	0.94*	−1.30*	540	811	20
$(TBA)_4[4,4'\text{-}dcb^-]_2Ru(NCS)_2$			518	740	88
$[4,4'\text{-}(LL)_2]RuCl_2$	0.59		598		
$[5,5'\text{-}(LL)_2Ru(CN)_2$	1.04*	−1.06*	578		<21
$(TBA)_4[5,5'\text{-}dcb^-]_2Ru(CN)_2$			520	715	75
$[5,5'\text{-}(LL)]_2Ru(NCS)_2$	0.95*	−0.95	585		
$(TBA)_4[5,5'\text{-}dcb^-]_2Ru(NCS)_2$			540	783	10
$[5,5'\text{-}(LL)]_2RuCl_2$	0.59		648		

[a] Transition metal compounds where 4,4′-(LL) is 4,4′-$(COOH)_2$-2,2′-bipyridine, 5,5′-(LL) is 5,5′-$(COOH)_2$-2,2′-bipyridine, 4,4′-dcb^- is 4,4′-$(COO^-)_2$−2,2′-bipyridine, 5,5′-dcb^- is 5,5′-$(COO^-)_2$-2,2′-bipyridine, and TBA is tetrabutylammonium cation. [b] Half-wave potentials in V *vs* SCE of the metal based III/II potential. The * indicates an anodic or cathodic peak potential for an irreversible oxidation or reduction process. Scan rate: 100 mV/s. [c] Reduction potentials in V *vs* SCE for the first ligand-based reduction. All reductions were found to be irreversible. [d] The maximum of the metal to ligand charge transfer absorption, ±2 nm. [e] The corrected room temperature photoluminescence maximum, ±6 nm. [f] Excited state lifetime obtained by laser flash photolysis or single-photon counting.

cellophane tape serves to determine the thickness of the TiO_2 coating as well as to mask an area of the electrode for ohmic contact to the conductive glass. Typically the TiO_2 geometric area was 1 cm^2. The electrodes were then dried in air for 30 min, followed by heating to 500 °C for 30 min in a Lindberg tube furnace. Samples were either used immediately for surface attachment reactions or stored in a desiccator until use.

Surface Attachment of Complexes. The inorganic compounds were attached to TiO_2 and SiO_2 surfaces by immersing the processed electrode in a $\sim 10^{-4}$ M ethanolic solution. The surface coverage of the complex reaches 95% of its limiting value after 24 h. During this time the electrode surface changes from white to the color of the attached dye. Surface converges were determined by spectroscopic measurement of the amount of complex in the $\sim 10^{-4}$ M ethanol solution before and after the attachment process. Surface coverages were independently verified spectroscopically by desorbing the complexes with pH 10 solution.[3]

Electrochemistry. Cyclic voltammetry was performed in 0.1 M TBAH/DMF solutions of the complexes using a standard three-electrode arrangement. A BAS Model CV27 potentiostat controlled either a Pt or glassy carbon working electrode, a Pt gauze counter electrode, and an SCE reference electrode separated from the solution by a frit.

Photoelectrochemistry. Photoelectrochemical measurements were performed in a two-electrode sandwich cell arrangement; the counter electrode was prepared by sputtering a thin layer of platinum onto the conductive side of a tin oxide electrode similar in size to the working electrode. The two electrodes were assembled into a "sandwich" arrangement with 0.5 M NaI and 0.05 M I_2 in propylene carbonate as electrolyte sandwiched between the Pt and TiO_2 electrodes. Current and voltage measurements were performed using a Keithley Model 617 digital electrometer having an input voltage burden of less than 3 mV.

The photoanodes were illuminated with either laser or lamp excitation. Broad-band lamp illumination involved placing the sample directly in the beam of a 150 W Xe lamp with a 400 nm Corning cut-on filter and an aqueous IR filter. This is referred to as "white light" excitation throughout the text. Photoaction spectrum were obtained with the 150 W Xe lamp coupled to an *f*/2 McPherson monochromator equipped with a holographic grating and a 3.2 mm fiber optic bundle. For laser excitation, the 457.9 or 488 nm line from a Coherent Model Innova 70A Ar ion laser was employed. The laser beam was passed through a band pass filter and expanded by 10×.

The stability of surface derivatized TiO_2 electrodes was studied by illuminating the photoanodes in the two electrode arrangement with either 200 mW/cm^2 of 488 nm light or 800 mW/cm^2 of broad-band excitation from an unfiltered 150 W Xe lamp. The photocurrent was monitored as a function of time for 2 h. Estimated indetermination in this experiment is ±10%. In general, the $[5,5'\text{-}(LL)]_2Ru(CN)_2$ and $[5,5'\text{-}(LL)]_2Ru(NCS)_2$ dyes are slightly more stable than their 4,4′-(LL) analogs. For example, after 2 h of white light excitation, the photocurrents of $[5,5'\text{-}(LL)]_2Ru(CN)_2$ and $[5,5'(LL)]_2Ru(NCS)_2$ sensitized electrodes decayed to 95% and 77% of the initial value, respectively. Under the same conditions, the photocurrents for both $[4,4'(LL)]_2Ru(CN)_2$ and $[4,4'(LL)]_2Ru(NCS)_2$ decayed to 70% of the initial value.

Optical Measurements. FTIR spectra were obtained with a Model IFS88 Bruker spectrometer on KBr pellets. Diffuse reflectance data were acquired on TiO_2 or KBr powder with a Nicolet 510 FTIR spectrometer equipped with a Spectra Tech diffuse reflectance accessory. Samples for reflectance IR measuremetns were prepared by stirring 20 mg of TiO_2 (Degussa P 25) in 5 mL of 10^{-4} M dye in ethanol for 2 h. The solutions were centrifuged, and the solid was washed with methanol and air dried.

Absorption, corrected emission spectra, and lifetimes were recorded with previously described apparatus.[3] Time resolved emission measurements from the sandwich cells were made with the sample 45° to the exciting wavelength. Scattered light was filtered with a potassium chromate solution filter. The instrument response function, IRF, was measured to be 14 ns with LUDOX colloidal SiO_2 as a light scatterer. All other details were as previously described.[3]

Excited State Absorption Spectroscopy. Transient absorbance signals were acquired following pulse excitation of 532 nm light by a Continuum Surelight Q-switched Nd:YAG laser (second harmonic, 4−6 ns fwhm, 10 mJ/pulse) using a pulsed Applied Photophysics 150 W Xe lamp as the monitoring light. The lamp was powered by an Applied Photophysics Model 04-122 power supply and pulsed with an Applied Photophysics Model 1410 pulsing unit. A shutter placed between the monitoring lamp and the cell was opened for 10 ms intervals to prevent PMT fatigue and sample photolysis. In addition, H_2O and glass filters were placed outside the lamp housing to prevent sample heating. The monitoring light was focused onto the sample, collimated after the sample, and finally focused onto the entrance slit of an Applied Photophysics *f*/3.4 grating monochromator. Transient signals were detected by a R446 PMT (Hamamatsu) optically coupled to the monochromator biased with a programmable Stanford PS 325 power supply. The transient signal was recorded with an optically triggered LeCroy 9450 digital storage oscilloscope interfaced to a 486 computer via GPIB. The absorption transients were plotted as $\Delta A = \log(I_0/I_t)$ vs time where I_0 was the monitoring light intensity prior to the laser pulse and I_t was the observed signal at delay time t. The laser oscillator and Q-switch, lamp, and shutter were all externally controlled with a digital logic circuit which allowed for synchronous timing. The instrument response function is estimated to be 21 ns using Rhodamine B (Exciton, Inc.) in ethanol as a standard.

Results

Spectroscopic Properties. For purpose of comparison, most of the spectroscopic, photophysical, and electrochemical measurements of *cis*-$[5,5'\text{-}(LL)]_2Ru(X)_2$ and *cis*-$[4,4'\text{-}(LL)]_2Ru(X)_2$ ($X = Cl^-$, CN^-, SCN^-) were performed in DMF solutions. The compounds were also soluble in water and alcohols and slightly soluble in acetonitrile. Relevant spectroscopic properties are summarized in Table 1, and the absorption spectra are shown in Figure 1.

Table 2. Infrared Frequencies of CN^- Stretching and CO_2^- Antisymmetric Stretching Bands[a]

	KBr		TiO_2	
compound[b]	ν(CN)	$\nu(CO_2^-)$	ν(CN)	$\nu(CO_2^-)$
$[4,4'\text{-(LL)}]_2Ru(CN)_2$	2085	1719	2081	1729, 1594
$Na_4[4,4'\text{-dcb}^-]_2Ru(CN)_2$	2077, 2059	1612		
$[4,4'\text{-(LL)}]_2Ru(NCS)_2$	2124	1706	2110	1730, 1600
$Na_4[4,4'\text{-dcb}^-]_2Ru(NCS)_2$	2126, 2116	1610		
$[4,4'\text{-(LL)}]_2RuCl_2$		1733		1725, 1600
$[5,5'\text{-(LL)}]_2Ru(CN)_2$	2077, 2050	1724	2093, 2056	1730, 1611
$Na_4[5,5'\text{-dcb}^-]_2Ru(CN)_2$	2070, 2062	1616, 1589		
$[5,5'\text{-(LL)}]_2Ru(NCS)_2$	2122	1726	2108	1731, 1610
$Na_4[5,5'\text{-dcb}^-]_2Ru(NCS)_2$	2124	1617, 1590		
$[5,5'\text{-(LL)}]_2RuCl_2$		1723		1734, 1611

[a] All frequencies are for strong or very strong bands in wavenumbers, ± 4 cm^{-1}. [b] Compounds where 4,4'-(LL) is 4,4'-$(COOH)_2$-2,2'-bipyridine, 5,5'-(LL) is 5,5'-$(COOH)_2$-2,2'-bipyridine, 4,4'-dcb^- is 4,4'-$(COO^-)_2$-2,2'-bipyridine, and 5,5'-dcb^- is 5,5'-$(COO^-)_2$-2,2'-bipyridine.

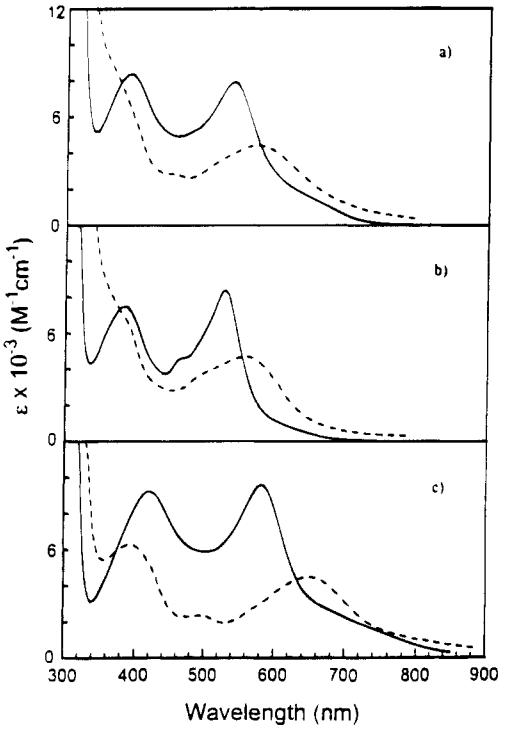

Figure 1. Absorption spectra of $[4,4'\text{-(LL)}]_2Ru(X)_2$ (—) and $[5,5'\text{-(LL)}]_2Ru(X)_2$ (- - -) in dimethylformamide: (a) X = SCN^-; (b) X = CN^-; (c) X = Cl^-.

The $[5,5'\text{-}(COO^-)_2bpy]_2Ru(X)_2^{4-}$ and $[4,4'\text{-}(COO^-)_2bpy]_2Ru(X)_2^{4-}$ species (X = CN^-, SCN^-) were found to be emitting in DMF solution at room temperature with visible excitation. Time resolved measurements demonstrate that the emission decays are exponential. Corrected emission maxima and lifetimes are reported in Table 1. Emission was also osberved for $[4,4'\text{-(LL)}]_2Ru(X)_2$ (X = CN^-, SCN^-), while no room temperature emission was observed for $[5,5'\text{-(LL)}]_2Ru(X)_2$ (X = CN^-, SCN^-) or any of the Cl^- complexes from 500 to 900 nm. We attempted to estimate the lifetime of the $[5,5'\text{-(LL)}]_2Ru(CN)_2$ by excited state absorption spectroscopy. However, the excited state lifetime was within the response function of our instrumentation.

Dye attachment to freshly prepared nanostructured TiO_2 films is 95% complete after 24 h in ethanol solution. On TiO_2 powder the dye was absorbed after 2 h. For TiO_2 films, independent of the molecular species, the final surface coverages on TiO_2 films is $(1.8 \pm 0.5) \times 10^{-7}$ mol/cm^2, Table 3. Treating the sensitizers as hard spheres with a diameter of 14 Å, a monolayer on a flat surface would correspond to $\sim 10^{-10}$ mol/cm^2. With this approximation, a surface roughness factor of 1300–2300 is calculated for these high surface area TiO_2 films. Compounds

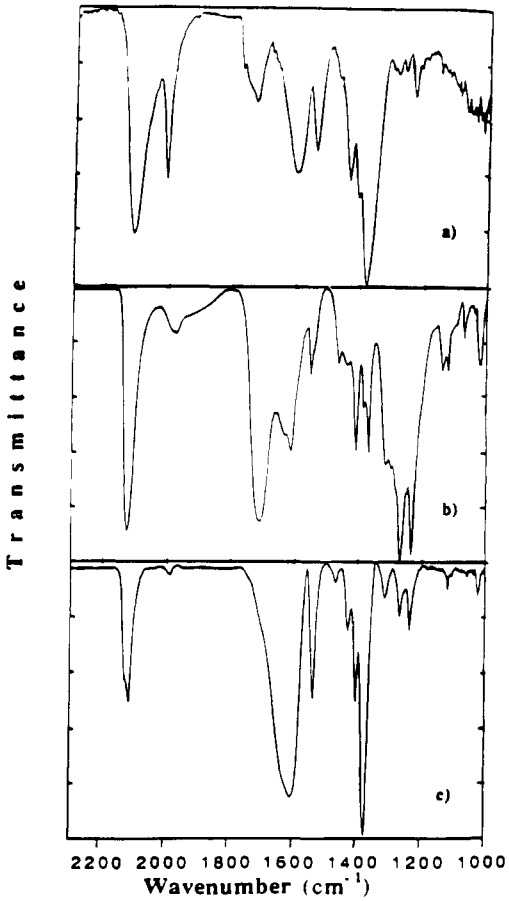

Figure 2. Infrared spectra of $[4,4'\text{-(LL)}]_2Ru(NCS)_2$ from 2300 to 1000 cm^{-1}. Panel a is the diffuse reflectance spectra of the compound attached to TiO_2, panel b is for the free compound in a KBr pellet, and panel c is for the anionic form of the compound with all four carboxylic groups deprotonated, $Na_4[(4,4'\text{-}(COO^-)_2\text{-}2,2'\text{-bipyridine})_2Ru(NCS)_2]$, in a KBr pellet.

which did not contain the carboxylic acid moieties, $Ru(bpy)_2(X)_2$ where X = CN^- or SCN^-, display no measurable surface attachment under the same conditions. The surface coverages were estimated by spectroscopic determination of the amount of dye absorbed and desorbed in basic solution as indicated in the Experimental Section.

Infrared spectra were recorded in the 4000–400 cm^{-1} region. Diffuse reflectance IR spectra of *cis*-$[4,4'\text{-(LL)}]_2Ru(NCS)_2$ anchored to TiO_2 powder is shown in Figure 2. By comparison with the free compounds in KBr, the frequencies for surface attached dyes could be assigned. Bands for the framework stretching modes of the coordinated 5,5'-(LL) and 4,4'-(LL) ligands appear in the 1600–1000 cm^{-1} range. Cyanide stretching bands for the coordinated CN^- and SCN^- ligands were

observed in the 2000−2150 cm^{-1} range for the free compounds. Broad stretches are observed in this region for the surface attached compounds which likely indicates different surface environments.

The idealized surface chemistry occurs by the reaction of surface hydroxyl groups with carboxylic acid groups to form ester linkages.[7,8] In general, the actual surface chemistry remains unknown and the carboxylate function could bind to Ti through several different modes, A−D.[9−11] An ester linkage

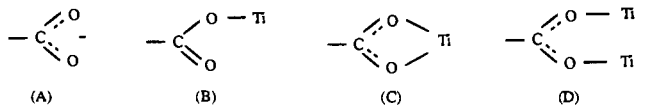

(B) has two inequivalent carbon-oxygen bonds and is expected to display the higher energy $\nu_{asym}(CO_2^-)$. We assign the peak near 1730 cm^{-1} (Figure 2a) to the ester linkage which is very close to that observed in the compound, [5,5′-$(CO_2C_2H_5)_2$-2,2′-bipyridine], $\nu_{asym}(CO_2^-)$ = 1721 cm^{-1}. The two peaks at 1598 and 1541 cm^{-1} are assigned to $\nu_{asym}(CO_2^-)$ possibly for A, C, and/or D. The framework stretching modes of the bipyridine ligands obscure the weak $\nu_{sym}(CO_2^-)$ which precludes us from distinguishing between these binding modes. The IR results do provide strong evidence for a surface ester bond and other carboxylato species. Spectra in the carboxylate region are virtually superimposable for all the surface attached 4,4′-(LL) and 5,5′-(LL) compounds. The CN^- stretching and CO_2^- antisymmetric stretching frequencies are summarized in Table 2.

Photoelectrochemical Properties. Figure 3 displays a plot of incident-photon-to-current-efficiency, IPCE(λ), for the six transition metal complexes anchored to TiO_2 electrodes. The measurements were made with an electrometer in a two electrode arrangement and a 0.5 M NaI/0.05 M I_2 propylene carbonate electrolyte solution. The IPCE(λ) is defined by eq I.

$$\text{IPCE}(\lambda) = \frac{(1.24 \times 10^3\ \text{eV·nm}) \times \text{photocurrent density } (\mu\text{A/cm}^2)}{\text{wavelength (nm)} \times \text{photon flux } (\mu\text{W/cm}^2)} \quad \text{(I)}$$

The figure demonstrates that the IPCE(λ) is dependent on the surface attached molecular compound. Maximum observed IPCE follows the trend [4,4′-(LL)]$_2$Ru(CN)$_2$ ~ [4,4′-(LL)]$_2$Ru(NCS)$_2$ > [4,4′-(LL)]$_2$Ru(Cl)$_2$ > [5,5′-(LL)]$_2$Ru(CN)$_2$ > [5,5′-(LL)]$_2$Ru(NCS)$_2$ > [5,5′-(LL)]$_2$Ru(Cl)$_2$. The same trend is observed in dimethylformamide and pH 2 water with NaI/I_2 electrolyte. If corrections are made for the absorbance of the tin oxide films, surface anchored [4,4′-(LL)]$_2$Ru(CN)$_2$ and [4,4′-(LL)]$_2$Ru(NCS)$_2$ convert photons into electrons with efficiencies >0.90 at individual wavelengths of light. The performance of the photoelectrochemical cells under white light illumination is given in Table 3. Short circuit photocurrent densities, I_{sc}, and open circuit photovoltages, V_{oc}, were measured as described in the Experimental Section. Current−voltage curves, from which the fill factors were calculated, are shown in Figure 4. The best performance is offered by the [4,4′-(LL)]$_2$Ru(NCS)$_2$ sensitizer.

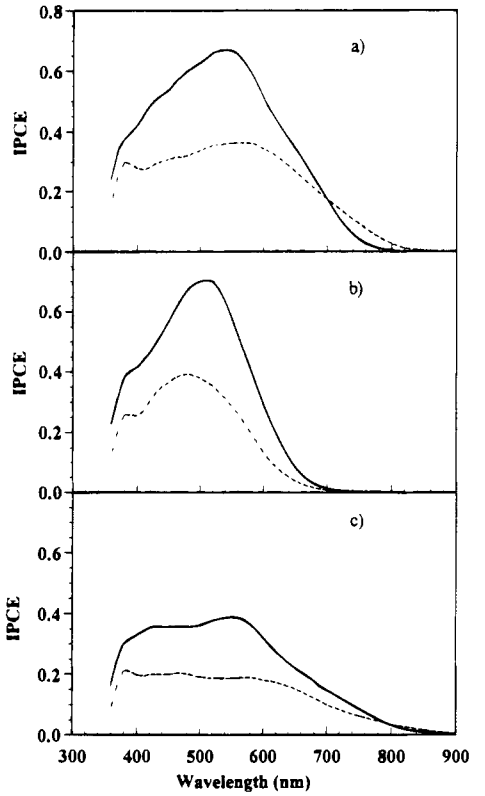

Figure 3. Photoaction spectra of the surface attached complexes [4,4′-(LL)]$_2$Ru(X)$_2$ (—) and [5,5′-(LL)]$_2$Ru(X)$_2$ (- - -) in propylene carbonate with NaI/I_2 electrolyte: (a) X = SCN^-; (b) X = CN^-; (c) X = Cl^-. The IPCE is defined under Results and further details are given in the Experimental Section.

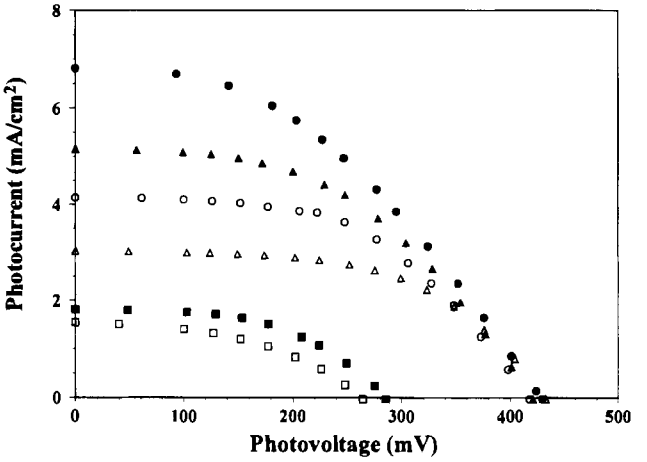

Figure 4. Photocurrent−voltage curves of the photoanodes under white light excitation. Circles: [4,4′-(LL)]$_2$Ru(NCS)$_2$ (filled) and [5,5′-(LL)]$_2$Ru(NCS)$_2$ (open). Triangles: [4,4′-(LL)]$_2$Ru(CN)$_2$ (filled) and [5,5′-(LL)]$_2$Ru(CN)$_2$ (open). Squares: [4,4′-(LL)]$_2$RuCl$_2$ (filled) and [5,5′-(LL)]$_2$RuCl$_2$ (open). Other details are given in the Experimental Section.

The effects of increased dye surface coverage on the photoelectrochemical properties was explored. Samples were prepared by exposing a TiO_2 electrode to an ethanolic Ru(II) solution for different periods of time. The total amount of dye absorbed on a given geometric electrode area was calculated spectrophotometrically in mol/cm^2, Γ. It is unknown how the

(7) (a) Fujihara, M.; Ohishi, N.; Osa, T. *Nature* **1977**, *268*, 226. (b) Fujihara, M.; Kubota, M.; Osa, T. *J. Electroanal. Chem.* **1981**, *81*, 379.
(8) (a) Anderson, S.; Constable, E. C.; Dare-Edwards, M. P.; Goodenough, J. B.; Hamnett, A.; Seddon, K. R.; Wright, R. D. *Nature* **1979**, *280*, 571. (b) Goodenough, J. B.; Dare-Edwards, M. P.; Campet, G.; Hamnett, A.; Wright, R. D. *Surf. Sci.* **1980**, *101*, 531. (c) Dare-Edwards, M. P.; Goodenough, J. B.; Hammett, A.; Seddon, K. R.; Wright, R. D. *Faraday Discuss. Chem. Soc.* **1980**, *70*, 285.
(9) Nakamoto, K.; McCarthy, P. J. *Spectroscopy and Structure of Metal Chelate Compounds*; John Wiley & Sons: New York, 1968.
(10) Thiele, K.-H.; Panse, M. *Z. Anorg. Allg. Chem.* **1978**, *441*, 23.
(11) Meyer, G. J.; Pfennig, B. W.; Schoonover, J. R.; Timpson, C. J.; Wall, J. F.; Kobusch, C.; Chen, X.; Peek, B. M.; Wall, C. G.; Ou, W.; Erickson, B. W.; Bignozzi, C. A.; Meyer, T. J. *Inorg. Chem.*, in press.

Table 3. Photoelectrochemical Properties of Sensitizers Attached to TiO_2

sensitizer[a]	max IPCE[b]	I_{sc} (mA/cm^2)[c]	V_{oc} (mV)[c]	ff[c]	$10^7\Gamma$ (mol/cm^2)[d]	LHE[e]
$[4,4'\text{-(LL)}]_2Ru(CN)_2$	0.706	5.18	421	0.48	1.3	0.914
$[4,4'\text{-(LL)}_2Ru(NCS)_2$	0.671	6.84	430	0.42	1.6	0.967
$[4,4'\text{-(LL)}]_2RuCl_2$	0.388	1.57	264	0.46	1.7	0.956
$[5,5'\text{-(LL)}]_2Ru(CN)_2$	0.393	3.05	433	0.56	2.2	0.849
$[5,5'\text{-(LL)}]_2Ru(NCS)_2$	0.366	4.17	418	0.52	1.6	0.714
$[5,5'\text{-(LL)}]_2RuCl_2$	0.204	1.84	285	0.52	1.4	0.758

[a] Sensitizer compounds where 4,4'-(LL) is 4,4'-$(COOH)_2$-2,2'-bipyridine and 5,5'-(LL) is 5,5'-$(COOH)_2$-2,2'-bipyridine. [b] Maximum incident photon to current conversion efficiency from Figure 2. [c] Short circuit photocurrent (I_{sc}), open circuit photovoltage (V_{oc}), and fill factors (ff) obtained in a sandwich cell arrangement with white light excitation from Figure 3. [d] Spectroscopically determined surface coverage of complex. [e] Light harvesting efficiency at wavelength of maximum IPCE.

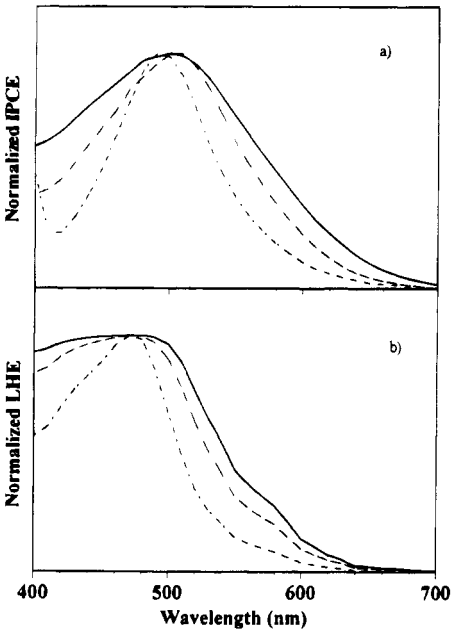

Figure 5. (a) Normalized photoaction spectra of $[4,4'\text{-(LL)}]_2Ru(CN)_2/TiO_2$ depicting spectral broadening with increasing surface coverage: (−·−·) 5.0×10^{-8} mol/cm^2; (− − −) 2.1×10^{-7} mol/cm^2; (—) 2.7×10^{-7} mol/cm^2. (b) Normalized light harvesting efficiency of surface attached $[4,4'\text{-(LL)}]_2Ru(CN)_2$ at the surface coverages indicated in (a). Theoretical light harvesting efficiency values were calculated on the basis of measured molar extinction coefficients in ethanol.

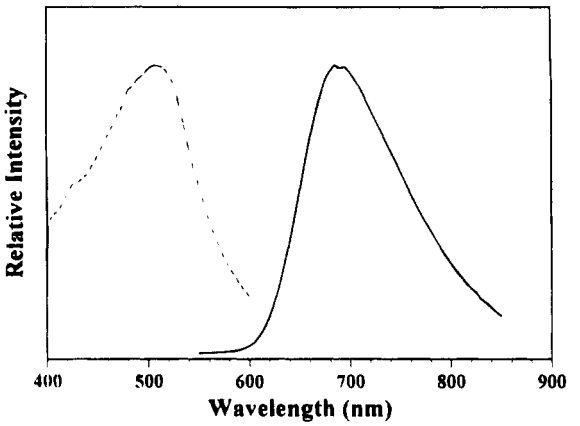

Figure 6. Corrected emission and excitation spectra of $[4,4'\text{-(LL)}]_2Ru(CN)_2/TiO_2$ in a sandwich cell configuration with I^-/I_2 dimethylformamide electrolyte.

dye molecules segregate within the nanostructured film. Shown in Figure 5a is the normalized photoaction spectrum, IPCE(λ), for $[4,4'\text{-(LL)}]_2Ru(CN)_2/TiO_2$ at the indicated surface coverages. The IPCE increases with surface coverage at these concentrations. Normalized spectra are shown to clearly demonstrate the broadening with increased surface coverage.

The absorptance, or absorption factor is defined as the radiant power absorbed by a system, P_{abs}, divided by the incident radiant power, P_0:[12]

$$\alpha = P_{abs}/P_0 \qquad \text{(II)}$$

In the photoelectrochemical literature, the absorption coefficient has been termed the Light Harvesting Efficiency, LHE, and we will use these terms interchangeably. When losses are due solely to absorption eq III applies, where T is the transmittance

$$\alpha = 1 - T = 1 - 10^{-A} \qquad \text{(III)}$$

and A is the absorbance.[12] Assuming Beer's law is applicable, the LHE(λ) can be related to the molar extinction coefficient by eq IV, where Γ is the surface coverage in mol/cm^2 and ϵ is the dye molar absorption coefficient in units of M^{-1} cm^{-1} at wavelength λ. LHE at the MLCT maximum and the measured surface coverages are given in Table 3. The normalized LHE for $[4,4'\text{-(LL)}]_2Ru(CN)_2$ at different surface coverages is given in Figure 5b, as calculated from eq IV. The molar extinction values were measured in ethanol, $\epsilon = 8200$ M^{-1} cm^{-1} at 490 nm.

$$\text{LHE}(\lambda) \equiv \alpha(\lambda) = 1 - 10^{-[1000(\text{cm}^3\text{L}^{-1})\cdot\epsilon(\text{mol}^{-1}\cdot\text{L}\cdot\text{cm}^{-1})\cdot\Gamma(\text{mol}\cdot\text{cm}^{-2})]} \qquad \text{(IV)}$$

Emission is observed for $[4,4'\text{-(LL)}]_2Ru(CN)_2/TiO_2$ and $[4,4'\text{-(LL)}]_2Ru(NCS)_2/TiO_2$ operating in the sandwich cell arrangement with I^-/I_2 in propylene carbonate, dimethylformamide or pH 2 water. The corrected emission and excitation spectra for $[4,4'\text{-(LL)}]_2Ru(CN)_2/TiO_2$ in a DMF iodide solution are shown in Figure 6. A weak emission from the TiO_2 substrate is observed, but the low quantum efficiency does not significantly affect the data reported here. Surface attached $[5,5'\text{-(LL)}]_2Ru(CN)_2$ and $[5,5'\text{-(LL)}]_2Ru(NCS)_2$ display no detectable emission under these conditions. In a three-electrode arrangement, the emission intensity is a function of the potential applied to the working photoanode. Typically the emission intensity increases by 40% when the potential is ramped from −0.5 to −1.2 V *vs* SCE. The spectral distribution of the emission is independent of the applied potential and the exciting wavelength within experimental error. A plot of relative emission intensity, open circuit photovoltage, and short circuit photocurrent versus light irradiance for a $[4,4'\text{-(LL)}]_2Ru(CN)_2/TiO_2$ derived sandwich cell is shown in Figure 7.

Nanosecond luminescence decay curves of $[4,4'\text{-(LL)}]_2Ru(CN)_2/TiO_2$ are shown in Figure 8. A luminescence decay of $[4,4'\text{-(LL)}]_2Ru(CN)_2$ attached to an insulating SiO_2 film in the sandwich cell arrangement is superimposed on the data for comparison. Luminescence decays from $[4,4'\text{-(LL)}]_2Ru(NCS)_2/TiO_2$ are sufficiently fast that quantitative analysis is precluded.

(12) Sheppard, N.; Willis, H. A.; Rigg, J. C. *Pure Appl. Chem.* **1985**, *57*, 105.

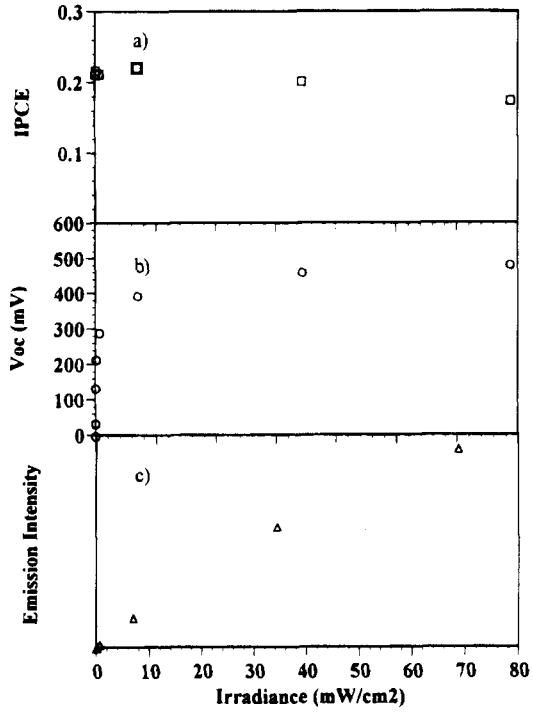

Figure 7. Performance of a $[4,4'\text{-}(LL)]_2Ru(CN)_2$ based regenerative cell as a function of irradiance at 457.9 nm. Figure 7a depicts decreasing efficiency at higher light flux, with a corresponding increase in photoluminescence intensity as monitored at 680 nm, Figure 7c. The open circuit photovoltage approaches a limiting value at high intensity, Figure 7b.

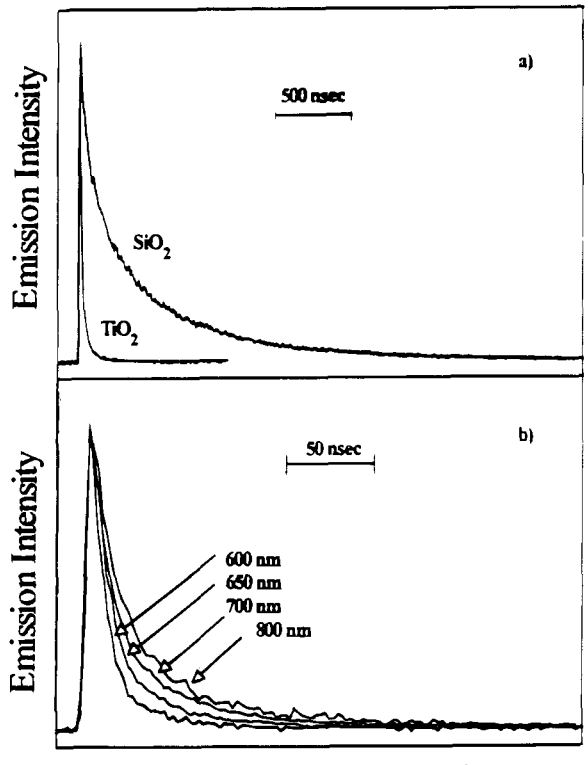

Figure 8. Time resolved luminescence spectra of $[4,4'\text{-}(LL)]_2Ru(CN)_2$. Panel a gives normalized decays for the compound attached to insulating SiO_2 and TiO_2 substrates. Panel b is the time resolved luminescence decay of $[4,4'\text{-}(LL)]_2Ru(CN)_2/TiO_2$ as a function of the monitoring wavelength. The samples were assembled in a sandwich cell configuration with I^-/I_2 propylene carbonate electrolyte and were illuminated with 100 μJ/pulse of ~200 ps duration at 460 nm.

Photoanodes which display low IPCE produce emission transients which are considerably longer than those shown in Figure 8. We have restricted this study to samples which display high IPCE. The decays from these samples are independent of the exciting irradiance from 5 to 100 μJ/pulse within experimental error. The decays are sensitive to the observation wavelength. Qualitatively, the decay rates become faster as the energy at which the emission is monitored increases, Figure 8b. Normalized uncorrected emission spectra 20 and 80 ns after a laser pulse are shown in Figure 9. The observed red shift in emission maximum is also observed for $4,4'\text{-}(LL)_2Ru(CN)_2$ anchored to SiO_2.

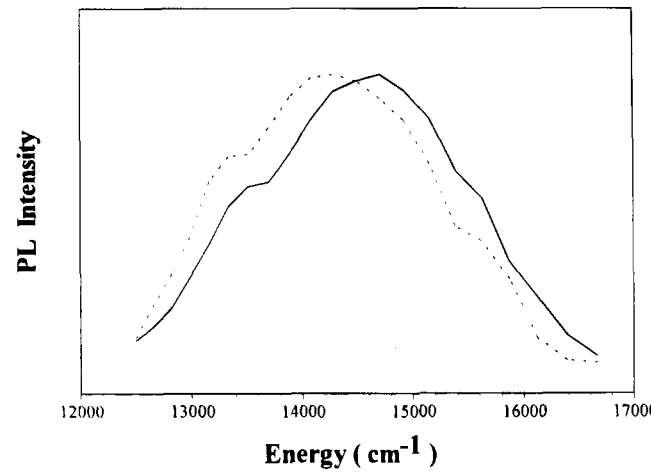

Figure 9. Uncorrected emission spectra of $[4,4'\text{-}(LL)]_2Ru(CN)_2/TiO_2$ at 15 (—) and (- - -) 80 ns after a 200 ps pulse. The samples were asssembled in a sandwich cell configuration with I^-/I_2 propylene carbonate electrolyte and were illuminated with 100 μJ/pulse at 460 nm.

The temporal data cannot be satisfactorily fit to a single rate constant. A sum of two or in some cases even three exponentials is needed to adequately describe these complex kinetics. The data can be satisfactorily fit to the William–Watts or Kohlrausch function, eq V.[13] In this equation, the parameter β

$$I(t) = \alpha \exp\left(-\frac{t}{\tau}\right)^{\beta} \qquad \text{(V)}$$

has a value between zero and unity which can be related to the width of an underlying Levy distribution of relaxation rates and τ is the lifetime at the maximum amplitude of the distribution. The mean lifetime, τ_{WW}, is the first moment of the Kohlrausch function, eq VI.[13c] In principle, the electron injection rate can

$$\tau_{WW} = \left(\frac{\tau}{\beta}\right)\Gamma\left(\frac{1}{\beta}\right) \qquad \text{(VI)}$$

be determined from the data presented in Figure 8a. The main assumptions are that electron transfer to the conduction band is the only quenching mechanism present in the TiO_2 films not present in SiO_2 and that $k_r + k_{nr}$ is independent of the substrate. With these assumptions, the interfacial electron injection rate can be estimated by

$$k_{et} = k_2 = 1/\tau_{TiO_2} - 1/\tau_{SiO_2} \qquad \text{(VII)}$$

Mean lifetimes were calculated for SiO_2 with eq VI. The systematic deviation from sample to sample far outweighed the error in individual fits so an average of three representative SiO_2 samples is $\tau_{SiO_2} = 259 \pm 21$ ns and $\beta = 0.53 \pm 0.02$. An estimation of an average rate for TiO_2 is more problematic.

(13) (a) Kohlrausch, R. *Ann.* **1847**, *5*, 430. (b) Williams, G.; Watts, D. C. *Trans. Faraday Soc.* **1971**, *66*, 80. (c) Lindsey, C. P.; Patterson, G. D. *J. Chem. Phys.* **1980**, *73*, 3348.

Eighty percent of the emission decays within 20 ns and we cannot eliminate the possibility that the remaining 20% is from sensitizers which do not inject electrons. We therefore estimate $\tau_{TiO_2} = 20$ ns as an upper limit. With these lifetimes an electron transfer rate $>5.0 \times 10^7$ s^{-1} from excited 4,4′-$(LL)_2Ru(CN)_2$ to the TiO_2 surface is estimated, eq VII.

Discussion

Sustained conversion of light into electricity has clearly been demonstrated with this family of molecular photovoltaic devices. The overall goal of extending the spectral response of dye sensitized TiO_2 toward the red has been achieved. The [5,5′-$(LL)]_2RuCl_2$ and [5,5′-$(LL)]_2Ru(NCS)_2$ sensitizers show increased absorbance and appreciable photocurent response at low energy when compared to the corresponding compounds with the carboxylate groups in the 4,4′ positions of the bipyridine ligand. A disappointing fact, however, is that the 5,5′-based dyes are less efficient at converting higher energy photons to electricity. At individual wavelengths of blue light the 4,4′-based dyes typically display incident photocurrent efficiencies greater than 0.70, while the 5,5′-dyes are less than 0.40. It is not immediately apparent why these chemically similar compounds display such dramatically different electro-optical properties.

A key parameter of cell performance is the incident-photon-to-current efficiency, IPCE, which directly measures how efficiently *incident* photons are converted to electrons. The IPCE is the product of the quantum yield for charge injection (ϕ), the efficiency of collecting electrons in the external circuit (η), and the fraction of radiant power absorbed by the material or the "light harvesting efficiency" (LHE), eq VIII. This

$$\text{ICPE} = (\text{LHE})(\phi)(\eta) \qquad \text{(VIII)}$$

equation neglects reflective losses. To better understand the factors which influence IPCE on a molecular level, it is worthwhile to compare the three parameters in eq VIII.

Light Harvesting Efficiency. The LHE is more generally termed the absorptance or the absorption factor, α.[12] An absorptance of unity is ideal for a solar energy device as all the incident radiant power is collected. Figure 5b gives the theoretical LHE(λ) for a [4,4′-$(LL)]_2Ru(CN)_2$ device as a function of surface coverage based on eq IV. Note how the theoretical spectra broaden with increasing surface coverage, a prediction which is realized experimentally in the normalized photoaction spectra, Figure 5a. The lower molar extinction coefficients for the 5,5′ dyes results in a lower LHE, Table 1. At these surface coverages the maximum and integrated light harvesting efficiencies are closest to ideal for [4,4′-$(LL)]_2Ru(NCS)_2$ which explains why it performs more favorably than the [4,4′-$(LL)]_2Ru(CN)_2$ sensitizer under white light excitation. The large differences in IPCE between the 4,4′- and 5,5′-based dyes cannot be explained solely by the small changes in LHE.

Electron Collection Efficiency. A remarkable property of these devices is their ability to efficiently collect electrons through a thick porous colloidal semiconducting layer. Resistive losses within the nanostructured TiO_2 film are expected to be independent of the surface attached dye. Factors which influence the efficiency of collecting electrons in the external circuit (η) must include recombination of the injected electron with the oxidized dye or electron donor, k_3 in Scheme 1. Recombination of the injected electron should be, if anything, more efficient for the 4,4′-based dyes due to the higher surface concentration of oxidized donors produced by the larger photocurrent density. The redox potentials of corresponding 4,4′- and 5,5′-based dyes are nearly equivalent which assures that the driving force for reduction of the oxidized dye by the thermalized conduction band electron is the same. Therefore, the molecular level similarity of the dyes and similar energetics for k_3 allow us to conclude that η is not the cause of differences in IPCE. The preceding discussion leads to the conclusion that differences in neither LHE nor η can adequately explain the lower solar energy conversion efficiencies observed for the 5,5′-based dyes. Electron transfer from the excited dye to the TiO_2 surface must therefore be less efficient.

Electron Injection Quantum Yield. Electron transfer from the excited dye to the TiO_2 surface, k_2, will be an activationless process if there exists maximum overlap between the excited donor levels and the wide conduction band acceptor.[4] The rate of activationless electron transfer from dye molecules to semiconductor surfaces is ultrafast and a lower limit of $k_2 > 10^9$ s^{-1} has recently been measured.[14] The quantum yield for electron injection (ϕ) is given by

$$\phi = \frac{k_2}{k_2 + k_r + k_{nr}} \qquad \text{(IX)}$$

where k_r and k_{nr} are the radiative and nonradiative rate constants for the excited dye and k_2 is the electron injection rate (Scheme 1). The high corrected photon-to-current efficiency observed for the 4,4′-based dyes indicates that ϕ is close to unity. A lower ϕ for the 5,5′-based dyes would occur if radiative or nonradiative decay competes with electron injection.

A decreased electron transfer rate will occur if the electron injection process is activated. The key parameter is the energetic difference between the sensitizer excited state donor levels and the conduction band edge. Excited state redox properties can be estimated through standard equations[5a,b] which would require, in this case, the knowledge of the ground state redox properties and the free energy difference between the ground and ^{3}MLCT excited state of the sensitizer absorbed on TiO_2. As an approximation, electrochemical and spectroscopic data obtained in fluid solution can be used. In DMF solution, the [4,4′-$(LL)]_2Ru(CN)_2$ sensitizer displays a reversible Ru(III/II) wave and an excited state redox potential of ~ -1 V *vs* SCE can be obtained. The [5,5′-$(LL)]_2Ru(X)_2$ (X = CN^-, SCN^-) show poorly reversible Ru(III/II) waves (Table 1) and luminesce only in their anionic form. With these limitations an estimate of -0.8 V *vs* SCE can be considered given the lower energy of the π^* accepting orbitals of 5,5′-(LL) *vs* 4,4′-(LL). This value is comparable to our preliminary estimate of the conduction band edge in propylene carbonate.[15] Previously, we have used impedance measurements with Mott−Schottky analysis to estimate the conduction band edge in pH 2 water.[16] The conduction band edge under these conditions is sufficiently positive that electron injection is activationless for all the sensitizers. In aqueous electrolyte the 5,5′-based dyes consistently display less than half the maximum IPCE of the corresponding 4,4′-compounds. Therefore, an activated electron transfer process cannot explain the lower IPCE of the 5,5′-based dyes.

A decreased electron transfer rate will occur if electronic coupling between the dye and sensitizer is lowered. Surface vibrational studies indicate that the mode(s) of binding are the

(14) (a) Willig, F.; Eichberger, R.; Sundaresan, N. S.; Parkinson, B. A. *J. Am. Chem. Soc.* **1990**, *112*, 2702. (b) Eichberger, R.; Willig, F. *Chem. Phys.* **1990**, *141*, 159.
(15) Cao, F.; et al. Work in Progress.
(16) Schmidt, J.; Searson, P. C.; Heimer, T. A.; Meyer, G. J. Submitted for publication.

same for all sensitizers but suggest a distribution of sensitizer-surface interactions. The high energy asymmetric carboxylate stretch, $\nu(CO_2^-) = 1730 \pm 5$ cm^{-1}, indicates the presence of a covalent ester linkage. The other interactions are difficult to quantitate at this time. Each type of interaction should correspond to an appropriate electronic matrix element for the charge injection process. The process could be adiabatic for the sensitizers bonded via the ester linkage and non-adiabatic for molecules which are less effectively coupled to the surface. In support of this picture is the observation that the emission and excitation spectra for $[4,4'\text{-(LL)}]_2Ru(CN)_2$ anchored to TiO_2 most closely resemble the anionic form of the sensitizer in fluid solution.

We have estimated the electron injection rate from the photoluminescence decays of the sensitizers on TiO_2 and SiO_2 substrates operating in a sandwich cell arrangement. We view this approach with caution as the assumptions presented under Results are severe and a discrete value is calculated when a distribution of electron transfer rates seems far more likely. The fact that most of the initial intensity decays within 20 ns along with highly nonexponential kinetics, leads us to conclude that the calculated rate, $k_2 = 5 \times 10^7$ s^{-1}, represents a slower rate in a skewed distribution of electron injection rates. This rate is in reasonable agreement with literature data for Ru(II) polypyridyl compounds on metal oxide colloids and powders,[17] but seems inconsistent with the electro-optical properties of *cis*-$[4,4'\text{-(LL)}]_2Ru(H_2O)_2$. This compound has an excited state lifetime of a few picoseconds yet efficiently sensitizes TiO_2.[2c] Picosecond emission studies yield extremely fast excited state electron transfer rates to the TiO_2 surface, $k_2 > 10^9$ s^{-1}.[14b] However, this compound appears to bind to TiO_2 through Ru–O–Ti bonds,[18] and the photophysical measurements were performed under conditions where the reorganizational energies which accompany electron transfer are likely very different.

An interesting observation is the time dependent red shift in the luminescence spectrum of $[4,4'\text{-(LL)}]_2Ru(CN)_2$ anchored to SiO_2 and TiO_2. The energy change observed on our time scale is ~200 cm^{-1}. We observe no analogous energy shift in the temporal luminescence spectrum of surface attached $[4,4'\text{-(LL)}]\text{-}Ru(bpy)_2^{2+}$. Therefore, the energy shift is a result of specific interactions between the ambidentate CN^- ligands[19] and the oxide surface and is not due to dipole reorientation.[20] The broadened multiple ν_{CN} stretches in the infrared spectrum of the attached sensitizer reinforce this conclusion. While the nature of the surface interaction is presently not known, we do note that the cyanide ligand alone is not sufficient for surface attachment of the Ru(II) sensitizers although it is sufficient for the binding of $[Fe(CN)_6]^{4-}$.[21]

A significant electronic difference between the 4,4′- and 5,5′-based dyes is the magnitude of the energy gap which is, to a first approximation, the energetic difference between the metal based III/II redox potential and the π^* levels of the bipyridine ligands. In moving the carboxylate moieties from the 4,4′- to the 5,5′-positions of the bipyridine ligand, the energy of the π^* levels is lowered and the metal redox potentials are slightly changed, Table 3. The resultant smaller energy gap manifests itself in the red shifted absorption spectra of the corresponding 5,5′-based compounds. For MLCT excited states, the energy gap law is applicable which predicts that the rate of nonradiative decay, k_{nr}, increases exponentially with decreasing energy gap.[22] The fast absorption changes and lack of emission from the 5,5′-based dyes preclude us from measuring the rate of nonradiative decay. Excited state absorption measurements place a lower limit of $k_{nr} > 4.8 \times 10^7$ s^{-1} which is comparable to the estimated lower limit for the rate of electron injection. We therefore conclude that the 5,5′-based sensitizers are less efficient at converting visible photons into electrons because nonradiative decay of the excited states competes effectively with electron injection lowering ϕ in eq VIII.

Conclusion

Enhanced spectral sensitivity from Ru(II) polypyridyl photovoltaic devices has been accomplished by molecular level design and use of $5,5'\text{-}(CO_2H)_2\text{-}2,2'$-bipyridine ligands. Unfortunately, the enhanced response at longer wavelengths is offset by a lower photocurrent efficiency at shorter wavelengths. Surface vibrational measurements and photoluminescence studies strongly suggest a distribution of interactions between the sensitizers and the TiO_2 surface. We conclude that the low photocurrent efficiency observed with the 5,5′-based sensitizers is in part due to a lower quantum yield for electron injection. This conclusion is not encouraging for the prospect of developing efficient black Ru(II) polypyridyl sensitizers where, on the basis of energy gap considerations, the rate of nonradiative decay will compete even more effectively with electron injection. However, more time resolved optical data from samples displaying high photocurrent efficiencies in operational photovoltaic devices is required before this fascinating interfacial behavior can be fully rationalized.

Acknowledgment. This work was supported by the National Renewable Energy Laboratories (Grant NREL XAD-3-12114-04). We thank Keithley Instruments and the Hamamatsu Corp. for the generous donation of an electrometer and the photon counting apparatus. The Italian portion of this work was supported by the Ministero della Universita e della Ricerca Scientifica e Technologica and by the Consiglio Nazionale delle ricerche (Progetto Finalizzato Chimica Fine).

(17) (a) Hashimoto, K.; Hiramoto, M.; Lever, A. B. P.; Sakata, T. *J. Phys. Chem.* **1988**, *92*, 1016. (b) Sakata, T.; Hashimoto, K.; Hiramoto, M. *J. Phys. Chem.* **1990**, *94*, 3040.
(18) Umpathy, S.; Cartner, A. M.; Parker, A. W.; Hester, R. E. *J. Phys. Chem.* **1990**, *94*, 8880.
(19) (a) Peterson, S. H.; Demas, J. N. *J. Am. Chem. Soc.* **1976**, *98*, 7880. (b) Demas, J. N.; Addington, J. W.; Peterson, S. H.; Harris, E. W. *J. Phys. Chem.* **1977**, *81*, 1039. (c) Peterson, S. H.; Demas, J. N. *J. Am. Chem. Soc.* **1979**, *101*, 6571. (d) Kinniard, M. G.; Whitten, D. G. *Chem. Phys. Lett.* **1982**, *88*, 275. (e) Bignozzi, C. A.; Scandola, F. *Inorg. Chem.* **1984**, *23*, 1540. (f) Davila, J.; Bignozzi, C. A.; Scandola, F. *J. Phys. Chem.* **1989**, *93*, 1373.
(20) Marcus, R. A. *J. Phys. Chem.* **1990**, *94*, 4963.
(21) (a) Vrachnou, E.; Gratzel, M.; McEvoy, A. J. *J. Electroanal. Chem.* **1989**, *258*, 193. (b) Blackbourn, R. L.; Johnson, C. S.; Hupp, J. T. *J. Am. Chem. Soc.* **1991**, *113*, 1060. (c) Lu, H.; Prieskorn, J. N.; Hupp, J. T. *J. Am. Chem. Soc.* **1993**, *115*, 4927.
(22) Freed, K. F.; Jortner, J. *J. Chem. Phys.* **1970**, *52*, 6272.